Theor Chem Acc (2007) 118:81–87
DOI 10.1007/s00214-007-0246-1

REGULAR ARTICLE

Electronic excitation in a *syn*-tetrasilane: 1,1,2,2,3,3,4,4-octamethyltetrasilacyclopentane

Raül Crespo · Mari Carmen Piqueras · Josef Michl

Received: 21 November 2006 / Accepted: 12 December 2006 / Published online: 1 February 2007

Abstract We present a multistate complete active space second-order perturbation theory (MS-CASPT2) study of the low-lying valence excited states of a peralkylated tetrasilacyclopentane, *c*-($CH_2Si_4Me_8$) (**1**). The lowest-lying calculated valence excited states are located in the 37,400–50,500 cm^{-1} region, in perfect agreement with experimental observations, 38,600–50,000 cm^{-1}. The MS-CASPT2 results provide a very good description of the nature, intensity, and position of the observed absorption bands, including the recently detected fourth electronic transition. The computational results have been used as a benchmark for evaluating a time-dependent density functional theory (TD-DFT) procedure suitable for calculations on longer oligosilanes.

Keywords Oligosilanes · Excited states · CASPT2 · TD-DFT

1 Introduction

The electronic properties of oligosilanes and polysilanes are very sensitive to chain conformation, and this is reflected in their thermochromism [1–3], piezochromism [4], solvatochromism [5,6], and related properties [7,8]. A detailed analysis and assignment of electronic transitions of oligosilanes as a function of conformation are therefore important, but they are difficult. Many conformers are normally present simultaneously, and their absorption bands are broad and closely spaced [9].

Cyclic structures are frequently utilized to control oligosilane conformation and simplify the spectral analysis. The four-silicon chain of tetrasilanes is the shortest that can exhibit backbone conformerism, and the absorption [10] and photoelectron [11] spectra of a series of monocyclic tetrasilanes constrained by a chain of CH_2 groups to particular dihedral angles were used to examine conformational effects on the properties of the tetrasilane unit. More recently, a wider variety of tetrasilanes constrained by hydrocarbon chains of various kinds have been used to investigate the conformational dependence of tetrasilane electronic states across the whole range of dihedral angles, from the syn to the anti geometry [12,13]. Similar results are beginning to appear for longer oligosilanes [14–16].

The tetrasilane **1** (Fig. 1), whose four silicon atoms are likely to be forced into a syn-planar geometry by incorporation into a five-membered ring, is of special interest. This is both because in this compound it was possible to detect as many as four distinct low-energy electronic transitions [12], and because the weak first transition is shifted to unusually long wavelengths [10,12], presumably due to cyclic hyperconjugation through the Si–CH_2–Si moiety. It is known from the spectrum of the polymer $(-CH_2SiMe_2SiMe_2SiMe_2SiMe_2-)_n$ that the effect of such interaction can be significant [17].

The assignment of transitions in **1** [12] was based (1) on previous MS-CASPT2 calculations for the gauche conformer of decamethyl-*n*-tetrasilane [18], which however has a much larger backbone dihedral angle (54.5°

Contribution to the Fernando Bernardi Memorial Issue.

R. Crespo (✉) · M. C. Piqueras
Departament de Química Física, Universitat de València,
Dr. Moliner 50, 46100 Burjassot (València), Spain
e-mail: Raul.Crespo@uv.es

J. Michl (✉)
Department of Chemistry and Biochemistry,
University of Colorado, Boulder, CO 80309-0215, USA
e-mail: michl@eefus.colorado.edu

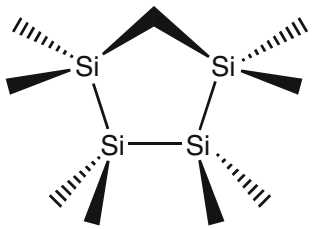

1

Fig. 1 Schematic representation of **1**

instead of 0°) and lacks the hyperconjugating CH_2 group, and (2) on TD-DFT results obtained at the B3LYP/DZ level for MM3 optimized geometry, which were corrected empirically by a constant 2,000 cm^{-1} shift. As a result, the assignment of the electronic transitions was not conclusive. There are several uncertainties in the understanding of the low-energy excited states of this cyclic tetrasilane, and it appeared very desirable to obtain a quantitative description of its low-lying valence excited states from high-level ab initio calculations. We now report such results, using the MS-CASPT2 method, which has already been shown to be applicable to the interpretation of the electronic spectra of oligosilanes [18–22], and we compare the results with those obtained using the TD-DFT method.

2 Computational details

The calculations were performed at the equilibrium geometry of **1**, obtained using second-order Møller–Plesset perturbation theory (MP2) as implemented in the Gaussian-03 program [23]. The geometry optimization employed Dunning's correlation consistent triple-ζ basis set (cc-pVTZ) [24] on all atoms and was constrained to the C_s point group symmetry, with the four silicon atoms in the *xy* plane. Frequency calculations performed at the MP2 level showed that the resulting C_s geometry is a minimum. Calculations using as a starting point a geometry with C_1 or C_2 symmetry led to the same C_s optimized geometry.

Electronic properties were computed from complete active self-consistent field (CASSCF) wave functions employing a generally contracted basis set of atomic natural orbitals (ANOs) obtained from Si(17s12p5d4f)/C(14s9p4d3f)/H(8s4p) primitive sets [25] using the Si[5s4p2d]/C[3s2p1d]/H[2s] contraction scheme. The reference wave function and the molecular orbitals were obtained from state average CASSCF calculations, where the average included all the A′ and A″ symmetry states of interest. All four 1s core orbitals of the silicon atoms were kept frozen, as determined by the ground-state Hartree–Fock (HF-SCF) wave function. After careful calibration calculations, the active space used was (5, 6), where the numbers specify the number of active orbitals belonging to the a′ and a″ irreducible representations of the C_s point group, respectively. The active space comprises the six σ and σ* Si–Si bond orbitals, two σ Si–C bond orbitals plus one σ* and two π* Si–C bond orbitals. The selection of the active space was made on the basis of our previous MS-CASPT2 studies on the electronic spectra of trisilane [19], *n*-tetrasilane [20,21], octamethyltrisilane [22], and decamethyl-*n*-tetrasilane [18]. The number of active electrons was set to ten.

To take into account the remaining correlation effects, particularly the correlation with the electrons of the Si–Me bonds, the CASSCF wave functions were employed as reference functions in a single-state second-order perturbation CASPT2 treatment [26]. The coupling of the CASSCF wave function via dynamic correlation was dealt with by means of the multistate CASPT2 (MS-CASPT2) method [27]. The MS-CASPT2 oscillator strengths were computed using perturbation modified CAS (PMCAS) reference functions [27] obtained as linear combinations of all CAS states involved in the MS-CASPT2 calculation. All calculations were performed with the MOLCAS-6 quantum chemistry program [28].

Electronic properties were also computed at the TD-DFT level using the B3LYP functional [29]. The calculations were carried out on the MP2 optimized geometry using the cc-pVTZ basis set for silicon and carbon atoms and the 6-311G basis set for the hydrogen atoms, and used the asymptotic correction approach of Casida and Salahub [30] as implemented in the NWChem program [31].

3 Results

3.1 Optimized geometry

The optimized minimum energy structure calculated at the MP2/cc-pVTZ level has a SiSiSiSi dihedral angle ω of 0°, compatible with the limited experimental evidence [10,11] and with previous MP2/TZ [11] and HF/3-21G* [32] results, but in contrast to MM3 results [12]. The latter method yielded two minima at $\omega = 15°$ and 21°, whose energy difference was of only 0.1 kcal/mol. The MP2/cc-pVTZ SiSiSi bond angle is 99.9°, similar to the MM3 results (100 and 99° at $\omega = 15°$ and 21°, respectively). The calculated SiSi bond distances are 2.367 and 2.369Å.

3.2 Orbitals

Figure 2 shows the natural orbitals obtained from the perturbation-modified CAS (PMCAS) wave functions of the valence excited states of **1** at the MS-CASPT2 level. Although the plane of the four silicon atoms is not a plane of molecular symmetry, the orbitals neatly fall into two categories. Those approximately symmetric with respect to the plane of the four silicon atoms shall be referred to as orbitals of σ type, and those approximately antisymmetric, as orbitals of π type.

All the orbitals are valence orbitals, and their nodal properties are those expected from Hückel considerations. This correspondence has been used for orbital labeling, which is based on the number of nodal surfaces. The occupied orbitals obtained at the DFT level correlate with those obtained at the MS-CASPT2 level.

The three highest occupied MOs, the HOMO (symmetry a′), the HOMO-1 (symmetry a″), and the HOMO-2 (symmetry a′) are all of σ type and correspond closely to simple Hückel expectations for σ(SiSi) bond orbitals. The orbital HOMO-3 (symmetry a″) is also of σ type, but it involves SiC bonds. The LUMO+1 (symmetry a′), LUMO+2 (symmetry a″) and LUMO+3 (symmetry a′) MOs are all of σ* type and correspond to simple Hückel expectations for σ*(SiSi) bond orbitals. The LUMO (symmetry a′) and LUMO+4 (symmetry a″) MOs are of π* type and fit Hückel expectations for the lowest-energy combinations of MOs formed from the antisymmetric combinations of localized σ*(SiC) antibonding orbitals of the lateral Si–CH_3 bonds on the silicon chain.

3.3 Electronic transitions

The vertical excitation energies and oscillator strengths of the first nine singlet valence excited states of **1** calculated at the MS-CASPT2 level and the TD-DFT (B3LYP) level using the MP2/cc-pVTZ optimized geometry are listed in Table 1, together with available experimental data [12] and previous TD-DFT/B3LYP/DZ//MM3 results [12]. The calculated electronic transitions are dipole-allowed and are located in four well-defined energy intervals near 37,000, 42,000, 47,000 and 50,000 cm^{-1}, which correspond neatly to the four experimentally observed bands.

Figure 3 compares the best experimental information available for the room-temperature UV absorption and magnetic circular dichroism (MCD) spectra of **1** with the MS-CASPT2 and TD-DFT simulations, assuming the spectral line shapes to be Gaussian functions with a

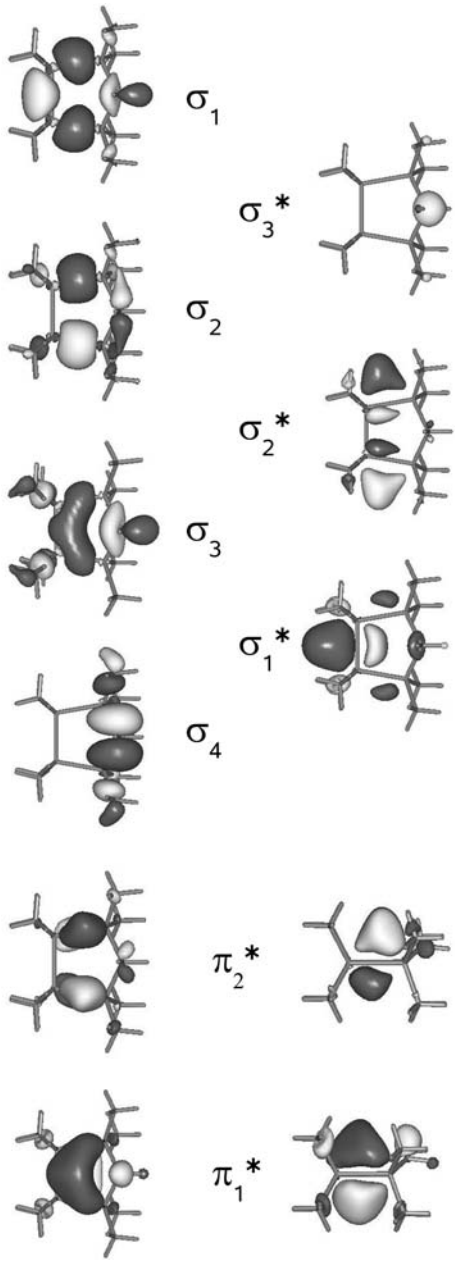

Fig. 2 Natural orbitals with occupation numbers close to unity obtained from the perturbation-modified CAS (PMCAS) wave functions of the valence-excited states of **1**. The isodensity surface value is 0.03

2,500 cm^{-1} full width at half-maximum, as in previous studies [18,19,21]. Solvent effects have been neglected.

In terms of natural orbitals (NO), the wave functions of the lowest energy excited states can be described as single electron promotions from an orbital that is nearly doubly occupied in the ground state to one that is nearly empty in the ground state, as the diagonalized excited state density matrices are characterized by two orbitals with occupancy very close to unity. For the higher

Table 1 MS-CASPT2 and TD-DFT/B3LYP/cc-pVTZ/cc-pVTZ/6-311G//MP2/cc-pVTZ vertical excitation energies (E, cm^{-1}) and oscillator strengths (f) of electronic transitions in **1**

Exp.[a]			MS-CASPT2			TD-DFT			TD-DFT[a]		
Band	E	$\varepsilon\times10^{-4}$	State[b]	E	f	State[b]	E	f	State[c]	E	f
1	38,600	0.05	$2^1A'(\sigma_1 \rightarrow \pi_1^*)$	37,400	0.005	$2^1A'(\sigma_1 \rightarrow \pi_1^*)$	37,400	0.0009	1^1B	41,200	0.004
2	42,200	0.31	$1^1A''(\sigma_2 \rightarrow \pi_1^*)$	41,800	0.003	$3^1A'(\sigma_1 \rightarrow \sigma_1^*)$	42,300	0.038	2^1A	46,500	0.02
			$3^1A'(\sigma_1 \rightarrow \sigma_1^*)$	41,900	0.141	$1^1A''(\sigma_2 \rightarrow \pi_1^*)$	42,600	0.0009	3^1A	46,900	0.03
3	46,100	0.72	$2^1A''$(mixed)[d]	47,000	0.375	$2^1A''(\sigma_2 \rightarrow \sigma_1^*)$	46,100	0.082	2^1B	50,600	0.05
4	49,300	~1.17	$4^1A'(\sigma_1 \rightarrow \sigma_3^*)$	48,700	0.049	$4^1A'(\sigma_1 \rightarrow \sigma_3^*)$	46,900	0.005	3^1B	51,300	0.12
			$3^1A''$(mixed)[d]	48,900	0.022	$3^1A''(\sigma_1 \rightarrow \sigma_2^*)$	47,600	0.028	4^1A	52,300	0.02
			$5^1A'(\sigma_3 \rightarrow \pi_1^*)$	50,100	0.399	$4^1A''(\sigma_2 \rightarrow \sigma_3^*)$	50,500	0.010	4^1B	54,100	0.04
			$4^1A''(\sigma_2 \rightarrow \sigma_3^*)$	50,400	0.080	$5^1A'(\sigma_3 \rightarrow \pi_1^*)$	50,700	0.037	5^1A	54,300	0.02
			$5^1A''(\sigma_4 \rightarrow \pi_1^*)$	50,500	0.023	$5^1A''(\sigma_4 \rightarrow \pi_1^*)$	50,900	0.033			

[a] Data from ref.12. TD-DFT values calculated at the TD-DFT B3LYP/DZ//MM3 level

[b] State label within C_s symmetry point group

[c] State label within C_2 symmetry point group

[d] $(\sigma_1 \rightarrow \sigma_2^*)$ and $(\sigma_2 \rightarrow \sigma_1^*)$ contributions

energy states, the picture becomes more complicated in that some of them are intrinsically multiconfigurational and their occupation numbers have significantly non-integral values.

The first calculated electronic transition, from the ground state to the $2^1A'$ excited state, occurs at 37,400 cm^{-1} . It is very weak and the calculated oscillator strength is only 0.005. This electronic transition corresponds to an excitation from the σ_1 HOMO to the π_1^* LUMO. The second and the third calculated electronic transitions are nearly degenerate. One is to the $1^1A''$ excited state calculated at 41,800 cm^{-1} and has a small oscillator strength (0.003). This electronic transition is from the σ_2 HOMO-1 to the π_1^* LUMO orbital. The much stronger other transition, nearly isoenergetic (41,900 cm^{-1}), is from the ground state to the $3^1A'$ excited state. This is one of the strongly allowed transitions, with a calculated oscillator strength of 0.141, and corresponds to an excitation from the σ_1 HOMO to the σ_1^* LUMO+1 orbital. This is the σ(SiSi)–σ^*(SiSi) transition that is considered the most characteristic of oligosilanes and polysilanes.

The next calculated electronic transition lies at 47,000 cm^{-1} and terminates in the $2^1A''$ excited state. It shows a strong oscillator strength of 0.375. This electronic transition is of multiconfigurational character, with contributions from promotions from the σ_1 HOMO to the σ_2^* LUMO+2 orbital and from the σ_2 HOMO-1 to the σ_1^* LUMO+1 orbital.

The next two electronic transitions, from the ground state to the $4^1A'$ and $3^1A''$ excited states, respectively, are very close in energy as they are calculated to lie at 48,700 and 48,900 cm^{-1}, respectively. They both exhibit relatively small oscillator strengths of 0.049 and 0.022, respectively. The first one ($4^1A'$) is due to an electron promotion from the σ_1 HOMO to the σ_3^* LUMO+3 orbital. The second one ($3^1A''$) is of multiconfigurational character. The contributing promotions are from the σ_1 HOMO to the σ_2^* LUMO+2 orbital and from the σ_2 HOMO-1 to the σ_1^* LUMO+1 orbital.

The transition to the $5\,^1A'$ excited state, calculated at 50,100 cm^{-1}, has a high oscillator strength (0.399) and corresponds to an excitation from the σ_3 HOMO-2 to the π_1^* LUMO orbital. Close in energy to this state there are two additional excited states of almost equal energy, $4^1A''$ and $5^1A''$, calculated at 50,400 and 50,500 cm^{-1}, respectively. The $4^1A''$ excited state is due to electron promotion from the σ_2 HOMO-1 to the σ_3^* LUMO+3 orbital, and the $5^1A''$ excited state is due to an electronic transition from σ_4 HOMO-3 to π_1^* LUMO. Transitions to other calculated excited states have an almost negligible oscillator strength, except for the $8^1A''$ and the $8^1A'$ excited states. The $8^1A''$ state, located at 55,700 cm^{-1}, has the highest oscillator strength (0.531) and the $8^1A'$ state, located at 56,500 cm^{-1}, has an oscillator strength of 0.136. The $8^1A''$ state corresponds to an excitation from the σ_4 HOMO-3 to the σ_3^* LUMO+3 and the $8^1A'$ state corresponds to the excitation from the σ_2 HOMO-1 to the π_2^* LUMO+4. These high energy states have not been included in Table 1, because there are neither experimental nor theoretical data to compare with.

The excited states calculated using the TD-DFT approach at the B3LYP/cc-pVTZ/cc-pVTZ/6-311G//MP2/cc-pVTZ level show energies very similar to those obtained at the MS-CASPT2 level. The calculated char-

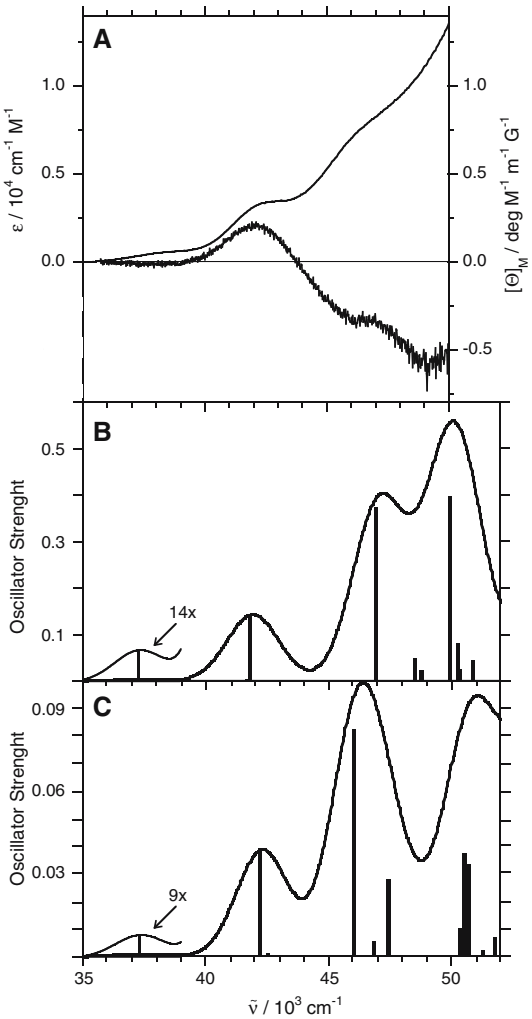

Fig. 3 UV absorption and MCD experimental spectra [12] **a**, MS-CASPT2 **b** and TD-DFT/B3LYP/cc-pVTZ/cc-pVTZ/6-311G//MP2/cc-pVTZ **c** simulation of the contributions of the low-energy valence states to the absorption spectrum of **1**, assuming a 2,500 cm^{-1} full width at half-maximum

acter of the electronic transitions also coincides, except for the $2^1A''$ and and $3^1A''$ excited states. These are the two excited states that showed multiconfigurational character at the MS-CASPT2 level. At the TD-DFT level, these electronic transitions are one-electron promotions, from the σ_2 HOMO-1 to the σ_1* orbital for the $2^1A''$ state, and from the σ_1 HOMO to the σ_2* orbital for the $3^1A''$ excited state. The main difference between MS-CASPT2 and TD-DFT methods are the values calculated for the oscillator strengths, with the latter being much lower.

4 Discussion

The difference in the SiSiSiSi dihedral angle of **1** obtained by ab initio and MM3 methods is somewhat disconcerting. We consider the ab initio results to be more reliable and believe that the dihedral angle of the silicon backbone in this compound is 0°. Except for the anticipated effects of cyclic hyperconjugation through the CH_2 group, it would therefore represent a good model for understanding the electronic structure of a general peralkylated *syn*-tetrasilane.

It has been concluded from a combination of absorption and MCD spectra [12] that at least four electronic transitions are present in the low-energy region below 50,000 cm^{-1}. The lowest energy transition 1, detected at 38,600 cm^{-1}, is extremely weak and hard to discern in the room-temperature absorption spectrum [12] shown in Fig. 3, but it is distinct in the low-temperature spectrum [10]. The negative MCD signal of this transition is also extremely weak. In spite of its weakness, this transition can be detected with confidence, because it does not overlap with others. Transition 2 is clearly present as a positive peak centered at 42,200 cm^{-1} in the MCD spectrum. Transition 3 appears at 46,100 cm^{-1} as a strong shoulder in absorption and as a strong negative shoulder in MCD. At higher energies, the absorption intensity increases further. Such end absorption suggests the presence of one or more additional transitions but does not permit an identification of the excitation energies. However, MCD shows a distinct negative peak at 49,300 cm^{-1}, which is assigned to transition 4. This contrasts with the other tetrasilanes investigated, which were constrained by longer hydrocarbon chains to six- to eight-membered rings and had larger SiSiSiSi dihedral angles, and whose MCD showed only gradually increasing negative intensity. The tetrasilane **1** was the only one in which four transitions were clearly identified. In the previously proposed assignments, based on TD-DFT B3LYP/DZ//MM3 calculations [12], agreement with the observed spectra was reasonable only after all calculated energies were reduced by 2,000 cm^{-1}. The results obtained in this paper at the TD-DFT B3LYP/cc-pVTZ/cc-pVTZ/6-311G//MP2/cc-pVTZ level are in better agreement with experimental results and no such empirical correction is needed. We assign the transitions based on our high-level ab initio MS-CASPT2 calculations.

Band 1 is attributed to a transition to a $1^1A'$ state calculated at 37,400 cm^{-1}, which is a HOMO to LUMO ($\sigma\pi^*$) excitation with a very low oscillator strength (0.005). Band 2 is assigned to a HOMO to LUMO+1 ($\sigma\sigma^*$) transition to the $3^1A'$ state calculated at 41,900 cm^{-1} with an oscillator strength of 0.141, which presumably hides a small contribution from a HOMO-1 to LUMO ($\sigma\pi^*$) transition to the $1^1A''$ state calculated at 41,800 cm^{-1} with an oscillator strength of only 0.003, too weak to be observed. Band 3 is mostly due to a transition to the $2^1A''$ state, calculated at 47,000 cm^{-1}

(oscillator strength, 0.375), of multiconfigurational character due to σσ* excitations from HOMO-1 to LUMO+1 and from HOMO-1 to LUMO+1. The fact that this intense transition involves excitation from the lower lying orbital HOMO-1 has not been stressed before, but it is in perfect agreement with the results obtained at the MS-CASPT2 level for *n*-tetrasilane [20,21] and decamethyl-*n*-tetrasilane [18]. Finally, the newly identified fourth observed band is interpreted as containing a large number of calculated overlapping transitions. Those to the $4^1A'$ and $3^1A''$ σσ* states at 48,700 and 48,900 cm^{-1} are relatively weak, with oscillator strengths of 0.049 and 0.022, respectively, and the main contribution to the observed absorption intensity is believed to be provided by the transition into the $5^1A'$ state, calculated at 50,100 cm^{-1} (oscillator strength, 0.399), and due to a HOMO-2 to LUMO σπ* excitation. Additional weak contributions are provided by transitions to the overlapping σσ* $4^1A''$ and σπ* $5^1A''$ states, located at 50,400 cm^{-1} (oscillator strength, 0.080) and 50,500 cm^{-1} (oscillator strength, 0.023). The remaining calculated high-energy states remain unobserved.

The σσ* or σπ* nature of the excited states is in good agreement with expectations based on a previously published correlation diagram [33]. The MS-CASPT2 results of Table 1 are in complete qualitative agreement with the previous picture, but the calculated energies are in much better agreement with observations and no empirical shift is needed.

The agreement between observed and calculated spectra is now excellent, and confirms our earlier conclusion [18–22] regarding the ability of the MS-CASPT2 procedure to calculate correctly the low-energy valence states of oligosilanes. Except for the now more reasonable values for oscillator strengths, there also is perfect agreement with the TD-DFT calculations. However, TD-DFT has difficulties describing correctly the excitation into the $2A''$ and $3A''$ states, given their multireference nature at the MS-CASPT2 level. The agreement is heartening for our current [12,34,35] and future efforts to use the TD-DFT procedure for longer oligosilanes, for which the MS-CASPT2 procedure becomes unmanageable. The results obtained in the present study at the MS-CASPT2 level could also serve as a benchmark for evaluating additional approximate methods that are less demanding of computer resources and suitable for applications to longer oligosilanes.

Acknowledgments This work was supported by Universitat de València, Generalitat Valenciana, Ministerio de Educación y Ciencia, European Commission, and the US National Science Foundation (CHE-0446688). NWChem Version 5.0, as developed and distributed by Pacific Northwest National Laboratory, was used to obtain some of these results.

References

1. Trefonas PT III, Damewood JR, West R, Miller RD (1985) Organometallics 4:1318
2. Harrah LH, Zeigler JM (1985) J Polym Sci Polym Lett Ed 23:209
3. Yuan C-H, West R (1988) Macromolecules 31:1087
4. Schilling FC, Bovey FA, Davis DD, Lovinger AJ, MacGregor RB Jr, Walsh CA, Zeigler JM (1989) Macromolecules 22:4645
5. Miller RD, Sooriyakumaran R (1988) Macromolecules 21: 3120
6. Oka K, Fujiue N, Dohmaru T, Yuan C-H, West R (1997) J Am Chem Soc 119:4074
7. Fujino M, Hisaki T, Matsumoto N (1995) Macromolecules 28:5017
8. Yuan C-H, West R (1997) J Chem Soc Chem Commun 1825
9. Fogarty HA, Casher DL, Imhof R, Schepers T, Rooklin DW, Michl J (2003) Pure Appl Chem 75:999
10. Imhof R, Teramae H, Michl J (1997) Chem Phys Lett 270:500
11. Fogarty HA, Tsuji H, David DE, Ottosson CH, Ehara M, Natatsuji H, Tamao K, Michl J (2002) J Phys Chem 106:2369
12. Fogarty HA, Imhof R, Michl J (2004) Proc Natl Acad Sci USA 29:10517
13. Tsuji H, Michl J, Tamao K (2003) J Organometallic Chem 685:9
14. Tsuji H, Fukazawa A, Yamaguchi S, Toshimitsu A, Tamao K (2004) Organometallics 23:3375
15. Tsuji H, Michl J, Tamao K (2003) Organomet Chem 685:9
16. MaziПres S, Raymond MK, Raabe G, Prodi A, Michl J (1997) J Am Chem Soc 119:6682
17. Isaka H (1997) Macromolecules 30:344
18. Piqueras MC, Crespo R, Michl J (2003) J Phys Chem A 107:4661
19. Piqueras MC, Crespo R, Michl J (2002) Mol Phys 100:747
20. Crespo R, Merchán M, Michl J (2000) J Phys Chem A 104:8593
21. Piqueras MC, Merchán M, Crespo R, Michl J (2002) J Phys Chem A 106:9868
22. Piqueras MC, Michl J, Crespo R (2006) Mol Phys 104:1107
23. Frisch MJ, Trucks GW, Schlegel HB, Scuseria GE, Robb MA, Cheeseman JR, Montgomery JA Jr, Vreven T, Kudin KN, Burant JC, Millam JM, Iyengar SS, Tomasi J, Barone V, Mennucci B, Cossi M, Scalmani G, Rega N, Petersson GA, Nakatsuji H, Hada M, Ehara M, Toyota K, Fukuda R, Hasegawa J, Ishida M, Nakajima T, Honda Y, Kitao O, Nakai H, Klene M, Li X, Knox JE, Hratchian HP, Cross JB, Bakken V, Adamo C, Jaramillo J, Gomperts R, Stratmann RE, Yazyev O, Austin AJ, Cammi R, Pomelli C, Ochterski JW, Ayala PY, Morokuma K, Voth GA, Salvador P, Dannenberg JJ, Zakrzewski VG, Dapprich S, Daniels AD, Strain MC, Farkas O, Malick DK, Rabuck AD, Raghavachari K, Foresman JB, Ortiz JV, Cui Q, Baboul AG, Clifford S, Cioslowski J, Stefanov BB, Liu G, Liashenko A, Piskorz P, Komaromi I, Martin RL, Fox DJ, Keith T, Al-Laham MA, Peng CY, Nanayakkara A, Challacombe M, Gill PMW, Johnson B, Chen W, Wong MW, Gonzalez C, Pople JA (2004) Gaussian 03, Revision C.02, Gaussian Inc., Wallingford
24. Kendall RA, Dunning TH Jr, Harrison RJ (1992) J Chem Phys 96:6796
25. Widmark PO, Persson BJ, Roos BO (1991) Theor Chem Acta 79:419
26. Andersson K, Malmqvist P-A, Roos BO (1992) J Chem Phys 96:1218
27. Finley J, Malmqvist P-A, Roos BO, Serrano-Andrés L (1998) Chem Phys Lett 288:299

28. Kalstrom G, Lindh R, Malmqvist P-A, Roos BO, Ryde U, Veryazov V, Widmark P-O, Cossi M, Schimmelpfenning B, Neogrady P, Seijo L (2003) Comput Mater Sci 28:222
29. Becke AD (1993) J Chem Phys 98:5648
30. Casida ME, Salahub DR (2000) J Chem Phys 113:8918
31. Bylaska EJ, de Jong WA, Kowalski K, Straatsma TP, Valiev M, Wang D, Apr BE, Windus TL, Hirata S, Hackler MT, Zhao Y, Fan P-D, Harrison RJ, Dupuis M, Smith DMA, Nieplocha J, Tipparaju V, Krishnan M, Auer AA, Nooijen M, Brown E, Cisneros G, Fann GI, Früchtl H, Garza J, Hirao K, Kendall R, Nichols JA, Tsemekhman K, Wolinski K, Anchell J, Bernholdt D, Borowski P, Clark T, Clerc D, Dachsel H, Deegan M, Dyall K, Elwood D, Glendening E, Gutowski M, Hess A, Jaffe J, Johnson B, Ju J, Kobayashi R, Kutteh R, Lin Z, Littlefield R, Long X, Meng B, Nakajima T, Niu S, Pollack L, Rosing M, Sandrone G, Stave M, Taylor H, Thomas G, van Lenthe J, Wong A, Zhang A (2006) NWChem, A computational chemistry package for parallel computers, Version 5.0, Pacific Northwest National Laboratory, Richland, Washington 99352–0999
32. Imhof R, Antic D, Davis DE, Michl J (1997) J Phys Chem A 101:4579
33. Albinsson B, Teramae H, Downing JW, Michl J (1996) Chem Eur J 2:529
34. Rooklin DW, Schepers T, Raymond-Johansson MK, Michl J (2003) Photochem Photophys Sci 2:511
35. Piqueras MC, Crespo R (2005) In: Auner N, Weis J (eds) Organosilicon chemistry VI. From molecules to materials vol. 1, pp 349